A Finite Fracture Mechanics approach to estimate the fatigue endurance limit of V-notched bars under multiaxial loading

International Journal of Fatigue 193 (2025) 108745

Contents lists available at ScienceDirect

International Journal of Fatigue

journal homepage: www.elsevier.com/locate/ijfatigue

# A Finite Fracture Mechanics approach to estimate the fatigue endurance limit of V-notched bars under multiaxial loading

Francesco Ferrian [a], Alberto Campagnolo [b,*], Alberto Sapora [a]

[a] Department of Structural, Geotechnical and Building Engineering, Politecnico di Torino, Corso Duca degli Abruzzi 24, 10129 Torino, Italy
[b] Department of Industrial Engineering, University of Padova, Via Venezia, 1, 35131 Padova, Italy

ARTICLE INFO

*Keywords:*
Finite Fracture Mechanics
Multiaxial fatigue
V-notched bar
Size effect

ABSTRACT

The current study aims to assess the high cycle fatigue strength of sharply V-notched bars under mixed mode I/III loading by applying the coupled Finite Fracture Mechanics (FFM) approach. FFM provides strength predictions by simultaneously satisfying a stress condition and an energy balance. A novel semi-analytical implementation of the FFM criterion is presented for the first time to account for a multiaxial fatigue loading by assuming that fracture early propagates along the notch bisector plane through a circumferential-shaped crack. To validate the model, fatigue strength predictions are then compared with a large variety of experimental data related to several metals, V-notch configurations and different multiaxial loading conditions. Although the adopted hypotheses are simplistic and do not fully encompass all the physical phenomena that occur in the multiaxial fatigue process, the approach reveals to be a reliable tool for obtaining semi-analytical fatigue endurance limit predictions useful for engineering design practice.

## 1. Introduction

Finite Fracture Mechanics (FFM) [1,2] is a coupled criterion that enables obtaining strength predictions for notched components by simultaneously satisfying a stress condition and the energy balance. The FFM criterion is thus able to overcome the drawbacks of the Linear Elastic Fracture Mechanics (LEFM) approach, which is limited to investigate the brittle failure behavior of largely cracked elements. Moreover, FFM is based on the assumption of finite crack advance in contrast to LEFM, which assumes continuous crack growth. This characteristic is common to other previously proposed nonlocal approaches, which can be grouped under the framework of Theory of Critical Distances (TCD) [3,4]. In contrast to TCD approaches, where the critical distance is solely considered as a material property, the FFM crack advance becomes a structural parameter, as it depends not only on the material but also on loading conditions and geometrical features under investigation. Consequently, FFM is able to catch the failure size effect of notched elements as the characteristic notch size changes [1]. Focusing on sharp V-notches under static loading conditions, FFM was initially applied to brittle materials under mode I loading by Leguillon [1], who compared strength predictions with experimental results on PMMA samples under three point bending. The same configuration was investigated by Carpinteri et al. [5] by comparing failure predictions with experimental data for polystyrene, duraluminum, and PMMA. Later, Carpinteri et al. [6] analyzed semi-infinite and finite-size V-notched plates subjected to remote uniaxial tension using the FFM approach. Mittelman and Yosibash [7] instead investigated crack onset in a sharply V-notched bar under torsion, considering finite crack propagation both in the notch bisector plane and in planes inclined at 45°. Applications of the FFM approach to notched configurations under combined mode I/III loading will be discussed in detail in Section 2.

Despite initially being proposed and applied only to static problems, FFM was later expanded to evaluate the fatigue endurance limit of structural elements. It is important to note that recent giga-cycle fatigue studies have observed fatigue failures in metallic materials beyond $10^7$ loading cycles [8,9]. These failures occurred when the stress range applied was below the conventional fatigue limit, suggesting that the traditional concept of the fatigue limit might have limitations and exceptions. Despite this, the fatigue limit continues to be a valuable parameter for the fatigue design of structural elements.

In the scientific literature, there is widespread acceptance that linear-elastic approaches can be reasonably implemented to assess the strength of structural components under fatigue endurance limit conditions, as this typically entails low strain and stress amplitudes. In this field, FFM has been applied to investigate the fatigue behavior of various

* Corresponding author.
*E-mail address:* alberto.campagnolo@unipd.it (A. Campagnolo).

https://doi.org/10.1016/j.ijfatigue.2024.108745
Received 3 October 2024; Received in revised form 9 November 2024; Accepted 29 November 2024
Available online 30 November 2024

**Nomenclature**

| | |
|---|---|
| $a$ | V-notch depth |
| $c$ | crack length at the notch root |
| $\ell_c$ | critical crack advancement |
| $R$ | net-section radius of the V-notched bar |
| $R_L$ | nominal load ratio |
| $\Delta K_I$ | mode I stress intensity factor (SIF) range |
| $\Delta K_{III}$ | mode III SIF range |
| $\Delta K_I^V$ | mode I notch SIF range |
| $\Delta K_{III}^V$ | mode III notch SIF range |
| $\Delta K_{I,th}$ | threshold value of the mode I SIF range for long cracks |
| $\Delta K_{III,th}$ | threshold value of the mode III SIF range for long cracks |
| $k_1$ | dimensionless shape function for mode I notch SIF of V-notched bar |
| $k_3$ | dimensionless shape function for mode III notch SIF of V-notched bar |
| $\Delta P$ | external axial load range |
| $\Delta M_b$ | external bending moment load range |
| $\Delta M_t$ | external torsion moment load range |
| $\alpha$ | ratio between $\Delta K_{III,th}$ and $\Delta K_{I,th}$ |
| $\omega$ | V-notch opening angle |
| $\rho$ | notch root radius |
| $(x, y, z)$ | cartesian coordinate system |
| $\Omega$ | nominal biaxiality ratio, i.e. $\Delta\tau/\Delta\sigma$ |
| $\varphi$ | phase shift angle between normal and shear stresses |
| $\lambda_I$ | mode I linear elastic eigenvalue |
| $\lambda_{III}$ | mode III linear elastic eigenvalue |
| $\sigma_{UTS}$ | ultimate tensile strength |
| $\Delta\sigma$ | nominal normal stress range |
| $\Delta\tau$ | nominal shear stress range |
| $\Delta\sigma_0$ | fatigue endurance limit range for plain samples under reversed axial loading |
| $\Delta\tau_0$ | fatigue endurance limit range for plain samples under reversed torsion loading |
| $\Delta\sigma_f$ | critical value of $\Delta\sigma$ at fracture initiation according to FFM |
| $\Delta\tau_f$ | critical value of $\Delta\tau$ at fracture initiation according to FFM |
| $\Delta\sigma_{f,exp}$ | experimental fatigue endurance limit for sharply V-notched bars under reversed mode I loading |
| $\Delta\tau_{f,exp}$ | experimental fatigue endurance limit for sharply V-notched bars under reversed mode III loading |
| $\Delta\sigma_{yy}$ | normal stress field at the tip of a V-notched bar under mode I loading |
| $\Delta\tau_{yz}$ | shear stress field at the tip of a V-notched bar under mode III loading |

structural configurations, considering several materials such as different types of steels, cast aluminum alloys and titanium alloys. Taking into account pure mode I loading conditions, the FFM approach was implemented to assess the fatigue strength of tensile plates weakened by a central circular hole [10,11] and crack [11], or by edge V- and U-notches [12], focusing on the crack/notch sensitivity phenomena under pure mode I loading. Furthermore, this approach has been applied to assess the fatigue endurance limit of 3D structures, such as spheroidal void in an infinite solid under remote tension [13], i.e. pure mode I. In that study, the failure size effect was investigated for different spheroid aspect ratios between 0.1 and 10 by considering an annular crack originating from the void's equator. Considering instead pure mode III loading conditions, Campagnolo and Sapora [14] analyzed the fatigue endurance limit behavior of V-notched bar subjected to torsion loading. The analysis was developed by assuming a shear stress-governed failure and a circumferential-shaped crack along the notch bisector plane. In this context, the aim of the present study is to extend for the first time the FFM approach to assess the fatigue endurance limit of V-notched components subjected to a multiaxial loading condition, generating a local mode I/III stress state. The study of multiaxial fatigue, in which mode I is combined with mode III, is crucial because it represents the most common scenario in practical engineering applications. The multiaxial local stress state arises from the complexity of both the component geometry (including the orientation of notches/defects as compared to the loading direction) and the in-service loading conditions, which typically do not consist of pure mode I, II, or III loads. Additionally, multiaxial loading conditions are the most challenging to analyze due to both a limited availability of experimental data in the literature and the lack of fatigue approaches which demonstrated to be reliable over a wide range of materials and geometrical/loading conditions [15].

## 2. Mixed mode I/III strength criteria

The multiaxial fatigue problem is a three-dimensional phenomenon that poses significant challenges in study due to its complexity. Indeed, the modeling of fatigue cracking behavior depends on a large number of factors, such as material type, notch configuration (i.e. the stress/strain distribution) and multiaxial loading conditions (e.g., loading ratio, biaxiality ratio and phase shift between the normal and shear stress components).

Various approaches have been developed to assess multiaxial fatigue life by analyzing how external loads combine to generate stresses and strains in a critical location. According to Socie and Marquis [15], these approaches can be classified in stress-, strain- or energy-based models. Typically, strain-based approaches are applied to investigate low cycle fatigue life, where significant plasticity may occur. In this framework, Brown and Miller [16,17] conducted combined axial and torsion tests considering a constant shear stress range. They proposed a criterion that considers both the shear and normal strains acting on the plane of maximum shear. Furthermore, they introduced the concept of Case A and Case B cracks. Cracks grow along the surface of the component in Case A, whereas they propagate into the depth in Case B. Fatemi and Socie [18], based on the work of Brown and Miller, suggested replacing the normal strain term with the normal stress. In this way, they included in their criterion the crack closure effects due to frictional forces induced by irregularity of the crack surface during shear loading. Several energy-based criteria have been proposed to investigate fatigue life under mixed-mode loading conditions since the work of Morrow [19]. In particular, the averaged Strain Energy Density (SED) criterion was applied to investigate the fatigue strength of several notched configurations subjected to different multiaxial loadings, e.g. [20,21,22]. According to this approach, the total strain energy density is evaluated within a structural volume whose dimension is a property of the material and loading mode.

Focusing on stress-based criteria, Gough and Pollard [23] proposed two empirical expressions, combining nominal normal and shear stresses, derived from an experimental campaign carried out on shafts subjected to in-phase bending-torsion loading:

$$\left(\frac{\Delta\sigma}{\Delta\sigma_0}\right)^2+\left(\frac{\Delta\tau}{\Delta\tau_0}\right)^2=1 \tag{1a}$$

$$\left(\frac{\Delta\sigma}{\Delta\sigma_0}\right)^2\left(\frac{\Delta\sigma_0}{\Delta\tau_0}-1\right)+\left(\frac{\Delta\sigma}{\Delta\sigma_0}\right)\left(2-\frac{\Delta\sigma_0}{\Delta\tau_0}\right)+\left(\frac{\Delta\tau}{\Delta\tau_0}\right)^2=1 \tag{1b}$$

where $\Delta\sigma$, $\Delta\tau$ represent the nominal normal and shear stress ranges and $\Delta\sigma_0$, $\Delta\tau_0$ are the fatigue endurance limits under reversed plane bending and torsional loadings, respectively. Eq. (1a) is valid for ductile

materials, whereas Eq. (1b) holds for brittle materials. Both expressions were formulated for plain samples under in-phase bending and torsion loadings, considering a load ratio $R_L = -1$. For notched components, Gough and Pollard [23] suggested using Eq. (1b) for both brittle and ductile materials, by substituting the notch fatigue endurance limits in place of the plain fatigue endurance limits. An empirical expression for out-of-phase loading conditions was proposed by Soon-Bok Lee (1985) [24]. Starting from the Gough and Pollard criterion expressed by Eq. (1a), they introduced an exponent dependent on the out-of-phase angle $\varphi$:

$$\left[\left(\frac{\Delta\sigma}{\Delta\sigma_0}\right)^{\mu}+\left(\frac{\Delta\tau}{\Delta\tau_0}\right)^{\mu}\right]^{\frac{1}{\mu}}=1 \quad \text{with} \quad \mu=2(1+\beta\sin\varphi) \tag{2}$$

where $\beta = 0.3$ for ductile materials and $\beta = 0.15$ for brittle materials based on experimental results related to several materials.

In addition to these empirical formulations, multiscale criteria were proposed by Dang Van [25] and Papadopoulos [26]. The fundamental concept behind these approaches is that crack initiation is a microscopic phenomenon occurring at the grain size. This idea is based on experimental observations of metal fatigue behavior, conducted on both single crystals and polycrystalline agglomerates. In particular, Papadopoulos [26] formulated a criterion valid also for out-of-phase loadings, closely resembling the arc of ellipse proposed by Gough and Pollard [23], as expressed by Eq. (1b):

$$\left(\frac{\Delta\sigma}{\Delta\sigma_0}\right)^2\left(\frac{2}{\sqrt{3}}\frac{\Delta\sigma_0}{\Delta\tau_0}-1\right)+\left(\frac{\Delta\sigma}{\Delta\sigma_0}\right)\left(2-\frac{2}{\sqrt{3}}\frac{\Delta\sigma_0}{\Delta\tau_0}\right)+\left(\frac{\Delta\tau}{\Delta\tau_0}\right)^2=1 \tag{3}$$

Additional criteria for evaluating crack initiation focus on assessing the stress state on a critical plane where fatigue damage reaches its maximum.

Findley [27] proposed determining the orientation of the critical plane based on a linear combination of the shear stress amplitude and maximum normal stress. Later on, Matake [28] defined the critical plane as the plane experiencing the maximum shear stress amplitude. Similar to Findley [27], Matake used a damage parameter based on evaluating a linear combination of the shear stress amplitude and the maximum normal stress on the critical plane. McDiarmid [28] and Susmel and Lazzarin [29] also defined the critical plane as the plane on which the shear stress amplitude attains its maximum. Specifically, McDiarmid [30] considered different material constants compared to Matake's model and incorporated the concept of Case A and Case B cracks introduced by Brown and Miller [16]. Susmel and Lazzarin [29], building on the theory of cyclic deformation in single crystals, proposed a criterion based on evaluating both the shear stress amplitude and the maximum normal stress acting on the critical plane. Another critical plane-based criterion was introduced by Carpinteri and Spagnoli [31], correlating the critical plane orientation with the averaged principal stress direction. More recently, Liu and Mahadevan [32] proposed that the critical plane not only depends on the stress state, but also on the material. Moreover, it may differ from the actual fracture plane, which is defined as the plane experiencing the maximum normal stress amplitude.

The crack front shape under mixed-mode I/III loadings was extensively investigated during the past decades. Under these loading conditions, the initial crack front tends to fragment into multiple cracks, called facets, thereby reducing mode III contribution and reaching a pure mode I condition. Moreover, as the crack front grows, some facets may merge resulting in a stepped fracture surface that gradually becomes coarser with crack growth [33]. Crack patterns under combined mode I/III loading were studied experimentally since the pioneering works by Sommer [34] and Knauss [35] who investigated facet nucleation in glass and polymer, respectively. Such complex crack patterns have also been observed in other materials, including metals [36,22,37], rocks [38] and polymers [39,40,41]. However, the characterization of the segmented crack front and the mechanism of facet nucleation remains a challenging problem. Furthermore, as the crack propagates, facets can merge and shield each other, leading to facet coarsening, as pointed out by Pham and Ravi-Chandar [42].

Geometrical features such as the distance between the facets and their twisting angles, are strongly dependent on loading conditions and considered material. Eberlein et al. [43] investigated crack onset and propagation by performing mixed mode I/III fatigue tests. Particularly, they analyzed how the magnitude of mode III affected various geometric features such as the projected length of the facets and their characteristic angles. Moreover, they observed experimentally that in some configurations the crack propagates continuously, without fragmentation in multiple cracks. This behavior was registered for a threshold value of the ratio between the mode III and mode I Stress Intensity Factors (SIF) $K_{III}/K_I < 0.57$. Cambonie and Lazarus [44] observed facets for $0.1 < K_{III}/K_I < 0.6$ in three-point bending tests conducted on PMMA samples. Crack growth under mixed-mode I/III loading was deeply investigated also by Pham and Ravi-Chandar [42,45]. For this purpose, they tested specially designed samples made of Homalite H-100 and glass evidencing the presence of facets for $K_{III}/K_I = 0.58$ [42] and $K_{III}/K_I = 0.001$ [45].

Facets nucleation under combined mode I/III loading was investigated through the numerical implementation of the FFM approach, by considering fracture plane as the one experiencing the maximum normal stress. Yosibash and Mittelman [46] predicted the initiation load of a single facet from a sharp V-notch edge, assuming an idealized crack shape. Doitrand and Leguillon [47] investigated the nucleation of a periodic array of facets from a primary crack, assuming a crack profile defined by stress isocontours. However, in both studies, the predicted loads at facet initiation were larger than those obtained for straight crack growth by implementing LEFM. Continuing within the FFM framework, the competition between straight crack propagation and facets nucleation from a primary crack front was investigated by Doitrand et al. [48]. This study accurately discussed the influence of the mode mixity ratio $K_{III}/K_I$ and T-stress magnitude on crack segmentation.

In this context, the present study investigates the fatigue behavior of sharply V-notched rounded bars subjected to combined axial/bending and torsion loadings. The geometry under investigation is depicted in Fig. 1. Key geometrical parameters include the notch opening angle $\omega$, the net-section radius $R$, and the notch depth $a$.

Given the complexity of the multiaxial fatigue problem discussed previously, this study assumes that crack initiation and early propagation occur along the notch bisector plane. This assumption is adopted to simplify the problem so that it can easily be treated in engineering design practice. The schematization of the circumferential-shaped crack in the cross-sectional area is depicted in Fig. 1. Under this hypothesis, a semi-analytical implementation of the FFM approach will be presented to assess fatigue endurance limit predictions.

## 3. FFM implementation

The FFM approach proposed by Leguillon [1] is able to provide strength estimations based on the simultaneous fulfillment of a pointwise stress condition and an energy balance. Both requirements must be satisfied over a critical distance, which becomes a structural parameter dependent on the material properties and the geometry under investigation. In this study, inspired by Gough and Pollard's formulation (Eq. (1a)), we chose to express the stress condition as an ellipse surface in the normal-shear stress space involving the expressions of the normal $\Delta\sigma_{yy}(x)$ and shearing $\Delta\tau_{yz}(x)$ stress field ranges referred to axial/bending and torsion loadings, respectively. The energy balance is written based on the simple empirical condition proposed by Hutchison and Suo [49], considering a circumferential-shaped crack. These two conditions yield:

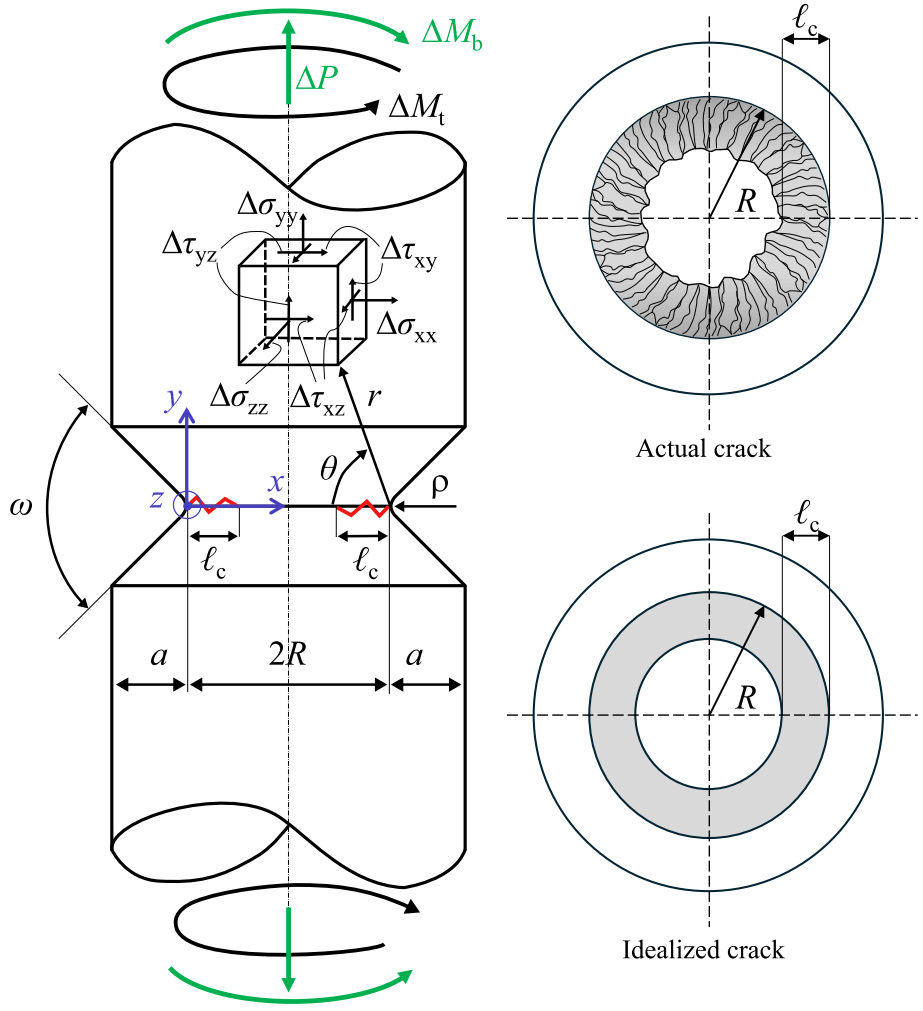


**Fig. 1.** Three-dimensional view and cross-sectional area schematization of a V-notched rounded bar under mixed-mode I/III loading. External loads are $\Delta P = \Delta\sigma{\cdot}\pi R^2$, $\Delta M_b = \Delta\sigma{\cdot}\pi R^3/4$ and $\Delta M_t = \Delta\tau{\cdot}\pi R^3/2$.

$$\begin{cases} \left(\dfrac{\Delta\sigma_{yy}(\ell_c)}{\Delta\sigma_0}\right)^2 + \left(\dfrac{\Delta\tau_{yz}(\ell_c)}{\Delta\tau_0}\right)^2 = 1 \\ \dfrac{1}{\pi R^2 - \pi(R-\ell_c)^2}\displaystyle\int_0^{\ell_c}\left[\left(\frac{\Delta K_I(c)}{\Delta K_{I,th}}\right)^2 + \left(\frac{\Delta K_{III}(c)}{\Delta K_{III,th}}\right)^2\right][2\pi(R-c)]\mathrm{d}c = 1 \end{cases} \tag{4}$$

where $\Delta K_I(c)$ and $\Delta K_{III}(c)$ represent the mode I and mode III ranges of the Stress Intensity Factors (SIFs) associated to a small crack $c$ originating from the notch root, respectively. $\Delta K_{I,th}$ and $\Delta K_{III,th}$ denote the corresponding mode I and mode III threshold values of the SIFs ranges. Following the approach proposed by Cornetti et al. [2], and thus considering an averaged stress condition, the FFM criterion can be reformulated as follows:

In Eqs. (4) and (5), we use a Cartesian coordinate system instead of cylindrical coordinates. This choice enables Eqs. (4) and (5), under pure mode III loading conditions, to revert to the formulations proposed by Campagnolo and Sapora [14] to investigate the torsional fatigue endurance limit of V-notched bars.

Both FFM approaches are defined by a system of two equations with two unknowns: the critical crack advancement $\ell_c$ and the axial/bending fatigue endurance limit range $\Delta\sigma_f$, implicitly embedded in the expression of the stress fields (Eq. (6a, b)) and the SIFs (Eq. (9a, b)). The torsional fatigue endurance limit can be expressed as $\Delta\tau_f = \Omega\bullet\Delta\sigma_f$, where $\Omega$ indicates the nominal biaxiality ratio. For a specific value of $\Omega$, the systems are solved by using the nonlinear system solver *fsolve* available in Matlab and considering a Trust-region-dogleg algorithm. This function enables us to solve a system of two equations by starting

$$\begin{cases} \dfrac{1}{\left[\pi R^2 - \pi(R-\ell_c)^2\right]^2}\left[\left(\dfrac{\int_0^{\ell_c}\Delta\sigma_{yy}(x)[2\pi(R-x)]\mathrm{d}x}{\Delta\sigma_0}\right)^2 + \left(\dfrac{\int_0^{\ell_c}\Delta\tau_{yz}(x)[2\pi(R-x)]\mathrm{d}x}{\Delta\tau_0}\right)^2\right] = 1 \\ \dfrac{1}{\pi R^2 - \pi(R-\ell_c)^2}\displaystyle\int_0^{\ell_c}\left[\left(\frac{\Delta K_I(c)}{\Delta K_{I,th}}\right)^2 + \left(\frac{\Delta K_{III}(c)}{\Delta K_{III,th}}\right)^2\right][2\pi(R-c)]\mathrm{d}c = 1 \end{cases} \tag{5}$$

from initial guesses for the variables and iteratively minimizing the sum of squares of the equations.

The implementation of the FFM approach requires the knowledge of the stress fields $\Delta\sigma_{yy}(x)$, $\Delta\tau_{yz}(x)$ and SIFs $\Delta K_I(c)$, $\Delta K_{III}(c)$ functions. As concerns the stress fields, according to the pioneering works by Williams [50] for mode I and by Qian and Hasebe [51] for mode III, we know that they are singular. The asymptotic expressions ahead the notch tip (along the notch bisector) are:

$$\Delta\sigma_{yy}(x) = \frac{\Delta K_I^V}{(2\pi x)^{1-\lambda_I}} \tag{6a}$$

$$\Delta\tau_{yz}(x) = \frac{\Delta K_{III}^V}{(2\pi x)^{1-\lambda_{III}}} \tag{6b}$$

where $\Delta K_I^V$ and $\Delta K_{III}^V$ are the mode I and mode III notch stress intensity factor (NSIF) ranges and $\lambda_I$, $\lambda_{III}$ denote the mode I and mode III eigenvalues. The NSIFs are defined as:

$$\Delta K_I^V = \lim_{x\to 0}\left[\Delta\sigma_{yy}(x)\cdot(2\pi x)^{1-\lambda_I}\right] \tag{7a}$$

$$\Delta K_{III}^V = \lim_{x\to 0}\left[\Delta\tau_{yz}(x)\cdot(2\pi x)^{1-\lambda_{III}}\right] \tag{7b}$$

$\lambda_{III}$ can be determined by exploiting the expression provided by Qian and Hasebe [51]:

$$\lambda_{III} = \frac{\pi}{2\pi-\omega} \tag{8a}$$

Meanwhile, the value of $\lambda_I$ is given by the smallest, real and positive root of the following equation:

$$\sin[(2\pi-\omega)\lambda_I] - \lambda_I \sin\omega = 0 \tag{8b}$$

They range between 0.5 for $\omega = 0°$ and 1 for $\omega = 180°$, when the singularity disappears and a straight edge is present. Values are reported every 30° in Table 1.

Considering the geometry under investigation, the NSIFs $\Delta K_I^V$ and $\Delta K_{III}^V$ were evaluated by Noda and Takase [52] and Zappalorto et al. [53], respectively. Noda and Takase calculated the mode I NSIF using the singular integral equation of the body force method. On the basis of notation (7*a*) for the NSIF, $\Delta K_I^V$ can be reformulated as:

$$\Delta K_I^V = k_1(\omega, a/R)a^{1-\lambda_I}\Delta\sigma \tag{9a}$$

where $\Delta\sigma$ is the nominal normal stress range on the net cross-sectional area. The shape functions $k_1$ were determined for different values of $\omega$ ranging between 15° and 90° and for $0 < a/R_{gross} < 0.9$, being $R_{gross} = R + a$. $k_1$ values are reported inAppendices A and B for axial and bending loadings, respectively. Note that for $a/R_{gross} \to 0$, the notch can be considered shallow and the shape functions revert to the case of a V-notch in a semi-infinite plate under tension.

Zappalorto et al. [53] evaluated the mode III NSIF through FEA and proposed the following formulation:

$$\Delta K_{III}^V = k_3(\omega, a/R)R^{1-\lambda_{III}}\Delta\tau \tag{9b}$$

where $\Delta\tau$ is the nominal shearing stress range on the net cross-sectional area. Accurate expressions of $k_3(\omega, a/R)$ were computed every 30° for $1/20 \le a/R \le 1$ using quadratic polynomials. For intermediate values of $\omega$ a linear interpolation is considered as presented in Appendix C.

Regarding the $\Delta K_I(c)$ and $\Delta K_{III}(c)$ functions, they can be approximated considering the following asymptotic expressions:

$$\Delta K_I(c) = \Lambda_I(\omega)\Delta K_I^V c^{\lambda_I - 0.5} \tag{10a}$$

$$\Delta K_{III}(c) = \Lambda_{III}(\omega)\Delta K_{III}^V c^{\lambda_{III} - 0.5} \tag{10b}$$

Eq. (10a) was proposed by Norio and Jiro [54] and very accurate $\Lambda_I$ values were provided lately by Philipps et al. [55] and Livieri and Tovo [56] for every 30° increment. Additionally, for intermediate angle values, Savruk and Rytsar [57] proposed an accurate analytical expression, with deviations from the $\Lambda_I$ values determined by Philipps et al. [55] being less than 1%. Considering $\alpha = \pi - \omega/2$ and the gamma function $\Gamma$, the approximate analytical expression for $\Lambda_I(\omega)$ in Eq. (10a) yields:

$$\Lambda_I(\omega) = \frac{(2\pi)^{\lambda_I}}{\pi\sqrt{2\psi}}\frac{\Gamma(\lambda_I/\psi)}{\Gamma(\lambda_I/\psi + 0.5)} \tag{11a}$$

where:

$$\psi = \frac{\pi\xi^2}{2} \tag{11b}$$

$$\xi = \sqrt{\frac{2\gamma + \sin(2\gamma)}{\gamma^2 - \sin^2(\gamma)}} \tag{11c}$$

$$\Gamma(\lambda_I/\psi) = \int_0^\infty t^{\lambda_I/\psi - 1}e^{-t}dt \tag{11d}$$

approximating function was proposed by Duan et al. [58] for $\Lambda_{III}$. According to definition (7*b*) for the NSIF, it yields:

$$\Lambda_{III}(\omega) = \sqrt{\frac{\pi}{\lambda_{III}(2\pi)^{2(1-\lambda_{III})}}} \tag{12}$$

Finally, it is worth noting that the FFM approach can be implemented by using the asymptotic expressions of the stress field and SIF ranges only when the finite crack advancement $\ell_c$ is small if compared to the net-section radius $R$. Otherwise, the stress gradient would be not negligible and should be included in Eqs. (4), (5).

**Table 1**
$\lambda_I$, $\lambda_{III}$, $\Lambda_I$ and $\Lambda_{III}$ values every 30°. Note that the values of $\Lambda_I$ and $\Lambda_{III}$ differ from those presented in Philipps et al. [55] and Duan et al. [58] due to the different definitions of the NSIFs expressed in Eqs. (7a, b).

| $\omega$ [°] | $\lambda_I$ | $\lambda_{III}$ | $\Lambda_I$ (from Philipps et al. [55]) | $\Lambda_I$ (from Savruk and Rytsar [57]) | $\Lambda_{III}$ (from Duan et al. [58]) |
|---|---|---|---|---|---|
| 0 | 0.5000 | 0.5000 | 1.000 | 1.000 | 1.000 |
| 30 | 0.5015 | 0.5455 | 1.005 | 1.002 | 1.041 |
| 60 | 0.5122 | 0.6000 | 1.017 | 1.013 | 1.097 |
| 90 | 0.5445 | 0.6667 | 1.059 | 1.052 | 1.176 |
| 120 | 0.6157 | 0.7500 | 1.161 | 1.150 | 1.293 |
| 150 | 0.7520 | 0.8571 | 1.394 | 1.384 | 1.472 |
| 180 | 1.0000 | 1.0000 | 1.985 | 1.995 | 1.773 |

## 4. Material properties

To implement the FFM approach and compare fatigue endurance limit predictions with experimental results available in the scientific literature, four material properties are necessary: $\Delta\sigma_0$ and $\Delta\tau_0$, representing the axial/bending and torsional fatigue endurance limits of the plain material; $\Delta K_{I,th}$ and $\Delta K_{III,th}$, denoting the threshold values of the mode I and mode III SIF ranges of the cracked material, for the same load ratio of the considered multiaxial data.

Regarding the fatigue endurance limits, they can be obtained by testing cylindrical plain samples and considering the stress range at $2\bullet10^6$ or $10^7$ cycles. Values of $\Delta\sigma_0$ and $\Delta\tau_0$ are available in the literature for different materials and will be presented and discussed in Section 5.

As concerns the values of $\Delta K_{I,th}$ and $\Delta K_{III,th}$, they are more complex to determine experimentally. Ideally, $\Delta K_{I,th}$ represents the value of the SIF range below which crack growth is not observed [59]. Various experimental techniques are available for determining the value of $\Delta K_{I,}$

th. For instance, these include the load reduction method, standardized by the ISO 12108 [60] and ASTM 647 [61] testing protocols. This method involves stepwise load reduction at a constant $R_L$, in a pre-cracked sample. Alternative procedures have been proposed such as the $K_{max}$ constant method [62] and the far-field cyclic compression procedure [63]. However, it is worth noting that the $\Delta K_{I,th}$ values obtained through these methods may differ due to the distinct mechanisms involved in the test procedure, related for instance to the fracture surface conditions and the plasticity induced at the crack tip [64,65]. Furthermore, Pearson [66] showed that small cracks may propagate even below the large-crack threshold defined by the ASTM test procedure.

Determining the threshold value of the mode III SIF range $\Delta K_{III,th}$ is extremely complex. Indeed, the comprehension of the mechanisms influencing the torsional fatigue phenomenon is significantly behind that of mode I, making it challenging to establish an analogous definition for mode III. Practical difficulties encountered in experimentally deriving $\Delta K_{III,th}$ are primarily associated with:

- mode transition which occurs before crack arrest. According to many researchers ([67,68,69,70]), fatigue crack propagation under torsion loadings typically results in a macroscopically flat (mode III) fracture surface for short cracks and high $\Delta K_{III}$ values. As the crack length increases, the crack growth rate decreases due to friction between the crack surfaces. Commonly, this frictional interference between crack faces leads to a change from a macroscopically flat (mode III) to a factory roof (mode I) type of fracture surface. This transition has been considered to define $\Delta K_{III,th}$ [68]. However, the threshold value thus defined is no longer comparable to that derived in mode I, as the crack continues to grow in a different mode and does not arrest. Moreover, this $\Delta K_{III,th}$ value is not a material property since the frictional contact between crack faces makes it dependent on the crack length;
- the extensive plastic region which can develop into small cracked bars;
- the threshold value varies depending on the tested sample geometry due to load dissipation on crack flanks and interference between crack faces. For instance, slit samples yield lower $\Delta K_{III,th}$ values with respect to pre-cracked samples in tension, while higher threshold values are obtained from V-notched rounded bars, even with identical notch tip radii as the slit specimens [70].

To overcome these difficulties in determining the $\Delta K_{III,th}$ value, several researchers attempted to establish a correlation between the threshold value of the mode III SIF range and the $\Delta K_{I,th}$ value through a correlation factor $\alpha$, such as $\Delta K_{III,th} = \alpha \bullet \Delta K_{I,th}$.

Regarding the coefficient $\alpha$, different values have been suggested in the literature based on analytical investigations and experimental results. Initially, Pook and Sharples [71] proposed $\alpha = 1.35$ based on analytical considerations and $\alpha = 1.25$ by considering $\Delta K_{III,th}$ values obtained from experimental tests on mild steels. Later, Pook [72] suggested implementing $\alpha = 1$ on the basis of a larger database of experimental tests conducted on metals. The same $\alpha$ value was proposed by Richard et al. [73] based on experimental findings from ferritic steel, which exhibited a propensity for mode III crack propagation. The same authors suggested a higher coefficient $\alpha = 1.6–3$ based on experimental results obtained on austenitic steel and Al 7075-T651, metals that were more prone to forming a factory roof type fracture surface. A lower value of $\alpha = 0.85$, always based on experimental results, was suggested by different authors [74,75,76]. The value of the coefficient $\alpha$ was derived also theoretically by Beretta and Murakami [77] by considering as mode III threshold condition the non-growth of mode I branched cracks. Finally, Tanaka [78], based on results obtained by torsional fatigue testing of steel bars, suggested using a different coefficient value for crack initiation ($\alpha = 1$) and propagation ($\alpha = 2–2.4$) thresholds.

Since there is no unanimous agreement in the scientific literature regarding the $\alpha$ value, in this study $\alpha = 1$ is considered, consistent with the choice made by Campagnolo and Sapora [14], who investigated mode III fatigue crack onset through the FFM approach.

## 5. Comparison with experimental data

To validate the accuracy of fatigue endurance limit predictions obtained through the FFM approach, under the assumptions discussed in the previous sections, a comprehensive database of 57 multiaxial fatigue datasets is used. The data are extracted from the scientific literature considering sharply V-notched rounded bars, subjected to multiaxial mode I/III fatigue loading with a load ratio $R_L = -1$. Several materials have been considered, including different types of steels (500 MPa $\leq \sigma_{UTS} \leq$ 1224 MPa), titanium alloys Ti-6Al-4 V ($\sigma_{UTS} = 978$ MPa) and cast iron grades (378 MPa $\leq \sigma_{UTS} \leq$ 485 MPa). Materials properties, along with experimental fatigue endurance limit ranges $\Delta\tau_{f,exp}$, $\Delta\sigma_{f,exp}$, and the main geometrical features, are reported in Table 2. A wide range of geometries ($0.13 \leq a/R \leq 1$ and $35° \leq \omega \leq 90°$) and multiaxial loading conditions ($0.53 \leq \Delta\sigma_{f,exp}/\Delta\tau_{f,exp} \leq 8.20$) have been investigated.

In axial-torsion fatigue tests, multiaxial testing machines are typically used, combining an axial actuator that applies a given force $\Delta P$ with a torsional actuator that applies a torque $\Delta M_t$ ([15,22]). These two actuators operate independently, enabling the desired values of $\Delta\sigma$ and $\Delta\tau$ to be achieved by adjusting the force and torque, with phase shift angles $\varphi$ if needed.

For bending-torsion loading conditions, multiaxial testing setups usually consist of two independent actuators connected to one end of the specimen via a load lever, while the other end of the specimen is fixed. The load applied by each actuator can be defined based on the target stresses and phase shift angles on the specimen's net section (for more details the Reader is referred to Refs. [15,79]).

Fatigue endurance limit data under in-phase axial-torsion loading for a low carbon steel were obtained by Quilafku [80] through testing samples with a notch opening angle $\omega = 35°$ and notch root radius $\rho$ of 0.2 mm and 0.4 mm. The axial and torsional fatigue endurance limits of the plain and notched samples were defined at $10^7$ cycles, while the values of $\Delta K_{I,th}$ and $\Delta K_{III,th}$ were not measured in the paper. To apply the FFM approach, we considered the $\Delta K_{I,th}$ value determined for this dataset by Susmel and Taylor [76]. In their study, Susmel and Taylor proposed an implementation of TCD to investigate torsional fatigue endurance limits in notched components. They determined the characteristic material length $L$ required for implementing the TCD approach through a numerical procedure, which involved calculating the stress field ahead of the notch tip using FE analyses. The characteristic material length was then determined by identifying the distance from the notch tip at which the stress equaled the plain fatigue endurance limit. The value of $\Delta K_{I,th}$ can thus easily be obtained from the value of the characteristic material length by considering the following relationship: $L = 1/\pi\,(\Delta K_{I,th}/\Delta\sigma_0)^2$. For this dataset, as well as the others, the value of $\Delta K_{III,th}$ is set equal to $\Delta K_{I,th}$, as previously discussed in Section 4.

Gough [81] generated a fatigue endurance limits dataset related to different steels by testing sharply V-notched bars (0.005 mm $\leq \rho \leq$ 0.03 mm) with $\omega = 55°$ and a ratio between the notch depth and the net radius $a/R = 0.13$. These data were obtained by Gough under several in-phase bending-torsion loading conditions ($0.53 \leq \Delta\sigma_{f,exp}/\Delta\tau_{f,exp} \leq 8.20$). Also in this case, fatigue endurance limits were defined at $10^7$ cycles, and the threshold values of SIF ranges were not reported. To implement the FFM approach, we considered the $\Delta K_{I,th}$ values determined for these materials by Susmel and Taylor [76], as described previously. Campagnolo and Sapora [14], investigating the mode III fatigue crack onset in V-notched bars, adopted a different value of $\Delta K_{I,th}$ for the steels tested by Gough [81]. They derived $\Delta K_{I,th}$ from an empirical equation proposed by Atzori et al. [82], which expresses $\Delta K_{I,th}$ as a function of the axial fatigue endurance limit of the plain material $\Delta\sigma_0$ and the ultimate tensile stress $\sigma_{UTS}$. It is worth noting that the formula proposed by Atzori et al. [82] provides a rough estimation of $\Delta K_{I,th}$

**Table 2**
Multiaxial fatigue **endurance** limit data ($R_L = -1$): material properties, main geometrical dimensions of the V-notched bars (Fig. 1), experimental fatigue **endurance** limits $\Delta\tau_{f,exp}$, $\Delta\sigma_{f,exp}$ under multiaxial loading conditions and deviations computed as: $[(\Delta\sigma_f - \Delta\sigma_{f,exp}) / \Delta\sigma_{f,exp}] \times 100$. For each experimental dataset $\Omega = \Delta\tau_{f,exp} / \Delta\sigma_{f,exp}$. For further information on experimental procedures and data scatter, please refer to the respective references.

| Material<br>Loading conditions[×] | Ref. | φ | $\sigma_{UTS}$ [MPa] | $\Delta\sigma_0$ [MPa] | $\Delta\tau_0$ [MPa] | $\Delta K_{th}$[#] [MPa$\sqrt{m}$] | $\omega$ [°] | $a/R$ | $\Delta\sigma_{f,exp}$ [MPa] | $\Delta\tau_{f,exp}$ [MPa] | FFM Eq. (4) Dev % | Avg-FFM Eq. (5) Dev % |
|---|---|---|---|---|---|---|---|---|---|---|---|---|
| Low carbon steel | [80] | 0° | 500 | 424 | 362 | 9.0* | 35 | 0.67 | 200 | 100 | −17.8 | −18.7 |
| A/T | | | | | | | | | 159 | 79 | 3.3 | 2.2 |
| 0.4 % C steel (normalized) | [81] | 0° | 639 | 664 | 414 | 12.4* | 55 | 0.13 | 153 | 280 | 25.5 | 15.9 |
| B/T | | | | | | | | | 240 | 215 | 21.4 | 15.5 |
| | | | | | | | | | 297 | 149 | 14.7 | 11.4 |
| | | | | | | | | | 332 | 103 | 7.9 | 5.8 |
| | | | | | | | | | 361 | 55 | 1.8 | 0.4 |
| 3 % Ni steel | [81] | 0° | 518 | 686 | 410 | 14.6* | 55 | 0.13 | 145 | 266 | 47.0 | 40.5 |
| B/T | | | | | | | | | 253 | 213 | 37.1 | 30.5 |
| | | | | | | | | | 343 | 167 | 16.7 | 13.4 |
| | | | | | | | | | 391 | 114 | 8.0 | 5.9 |
| | | | | | | | | | 418 | 51 | 3.5 | 2.1 |
| 3/3.5 % Ni steel | [81] | 0° | 712 | 704 | 534 | 21.6* | 55 | 0.13 | 351 | 307 | 41.5 | 34.2 |
| B/T | | | | | | | | | 429 | 217 | 35.5 | 31.2 |
| | | | | | | | | | 531 | 157 | 16.5 | 14.1 |
| | | | | | | | | | 572 | 80 | 10.9 | 9.3 |
| Cr-Va steel | [81] | 0° | 740 | 858 | 516 | 15.2* | 55 | 0.13 | 155 | 295 | 43.2 | 36.7 |
| B/T | | | | | | | | | 275 | 234 | 32.7 | 26.5 |
| | | | | | | | | | 344 | 177 | 21.1 | 17.5 |
| | | | | | | | | | 421 | 116 | 5.4 | 3.5 |
| | | | | | | | | | 422 | 56 | 7.2 | 5.7 |
| 3.5 % NiCr steel (normal impact) | [81] | 0° | 882 | 1080 | 704 | 19.4* | 55 | 0.13 | 206 | 376 | 42.4 | 36.6 |
| B/T | | | | | | | | | 340 | 291 | 37.3 | 30.8 |
| | | | | | | | | | 456 | 228 | 17.2 | 13.8 |
| | | | | | | | | | 522 | 154 | 7.9 | 5.9 |
| | | | | | | | | | 582 | 74 | −0.7 | −2.1 |
| 3.5 % NiCr steel | [81] | 0° | 883 | 1018 | 648 | 17.9* | 55 | 0.13 | 336 | 295 | 26.8 | 20.7 |
| (low impact) | | | | | | | | | 397 | 199 | 24.2 | 20.6 |
| B/T | | | | | | | | | 448 | 134 | 16.1 | 13.9 |
| | | | | | | | | | 471 | 64 | 13.1 | 11.5 |
| NiCrMo steel | [81] | 0° | 1224 | 1188 | 686 | 18.2* | 55 | 0.13 | 208 | 390 | 35.5 | 25.3 |
| B/T | | | | | | | | | 340 | 295 | 28.9 | 22.9 |
| | | | | | | | | | 475 | 248 | 5.4 | 2.4 |
| | | | | | | | | | 506 | 151 | 4.9 | 2.9 |
| | | | | | | | | | 531 | 73 | 2.1 | 0.7 |
| Ti-6Al-4 V | [79] | 0° | 978 | 1016 | 847 | 21.0+ | 90 | 1.0 | 208 | 361 | 28.6 | 14.4 |
| B/T | | 90° | | | | | | | 202 | 350 | 32.7 | 18.0 |
| A/T | [22] | 0° | 978 | 951 | 777 | 16.9+ | 90 | 1.0 | 188 | 113 | 43.6 | 34.3 |
| | | 90° | | | | | | | 192 | 115 | 40.3 | 31.2 |
| EN-GJS400 | [84] | 0° | 378 | 301 | 291 | 14.9+ | 90 | 0.7 | 148 | 148 | 27.9 | 16.1 |
| A/T | | 90° | | | | | | | 165 | 165 | 14.5 | 4.0 |
| | | 0° | | | | | | | 199 | 118 | 7.2 | −0.7 |
| | | 90° | | | | | | | 172 | 103 | 24.4 | 15.3 |
| 39NiCrMo3 | [83] | 0° | 995 | 630 | 531 | 26.3+ | 90 | 0.7 | 299 | 299 | 13.6 | 3.5 |
| A/T | | 90° | | | | | | | 234 | 234 | 45.3 | 32.3 |
| | | 0° | | | | | | | 359 | 216 | 6.7 | −0.9 |
| | | 0° | | | | | | | 246 | 394 | 11.0 | −0.9 |
| C40 | [20] | 0° | 715 | 528 | 392 | 23.5+ | 90 | 0.7 | 202 | 202 | 46.7 | 33.4 |
| A/T | | 90° | | | | | | | 199 | 199 | 48.7 | 35.2 |
| EN-GJS-600 | [85] | 0° | 485 | 340 | 320 | 13.3+ | 60 | 0.4 | 147 | 147 | 10.8 | 5.1 |
| A/T | | 90° | | | | | | | 186 | 186 | −12.5 | −17.0 |
| EN-GJS-450 | [85] | 0° | 476 | 360 | 300 | 12.6+ | 60 | 0.4 | 131 | 131 | 18.1 | 12.1 |
| A/T | | 90° | | | | | | | 172 | 172 | −10.1 | −14.7 |
| EN-GJS-400 | [85] | 0° | 378 | 290 | 280 | 14.3+ | 90 | 0.7 | 139 | 139 | 30.4 | 18.4 |
| A/T | | 90° | | | | | | | 161 | 161 | 12.3 | 2.0 |
| | | 0° | | | | | | | 173 | 104 | 18.4 | 9.7 |
| | | 90° | | | | | | | 158 | 95 | 29.6 | 20.1 |

[×] A, axial; B, bending; T, torsion.
[#] $\Delta K_{th} = \Delta K_{I,th} = \Delta K_{III,th}$ since we considered $\Delta K_{III,th} = \alpha \bullet \Delta K_{I,th}$ with $\alpha = 1$, as discussed in Section 3.
[*] $\Delta K_{I,th}$ has been derived by Susmel and Taylor [76].
[+] $\Delta K_{I,th}$ has been determined by assuming the crack case equivalent to the sharp V-notch case with $\omega = 90°$ under mode I loading.

suitable for engineering estimations, as clarified in the original paper from the authors. For the sake of completeness, Fig. 2 illustrates the experimental data obtained by Gough [81] by testing V-notched bars under pure torsion, and the fatigue endurance limit predictions provided by the avg-FFM approach defined by Eq. (5), considering pure mode III loading conditions. Specifically, Fig. 2a compares theoretical predictions and experimental results considering the material properties determined by Susmel and Taylor [76], while in Fig. 2b the material properties implemented by Campagnolo and Sapora [14] are considered. Discrepancies between theoretical predictions and experimental results are comparable in both scenarios.

Experimental fatigue data [83,84,22,79] were obtained by testing 90° V-notched bars, with a notch root radius $\rho = 0.1$ mm, under both in-phase and out-of-phase axial-torsion [83,84,22] and bending-torsion

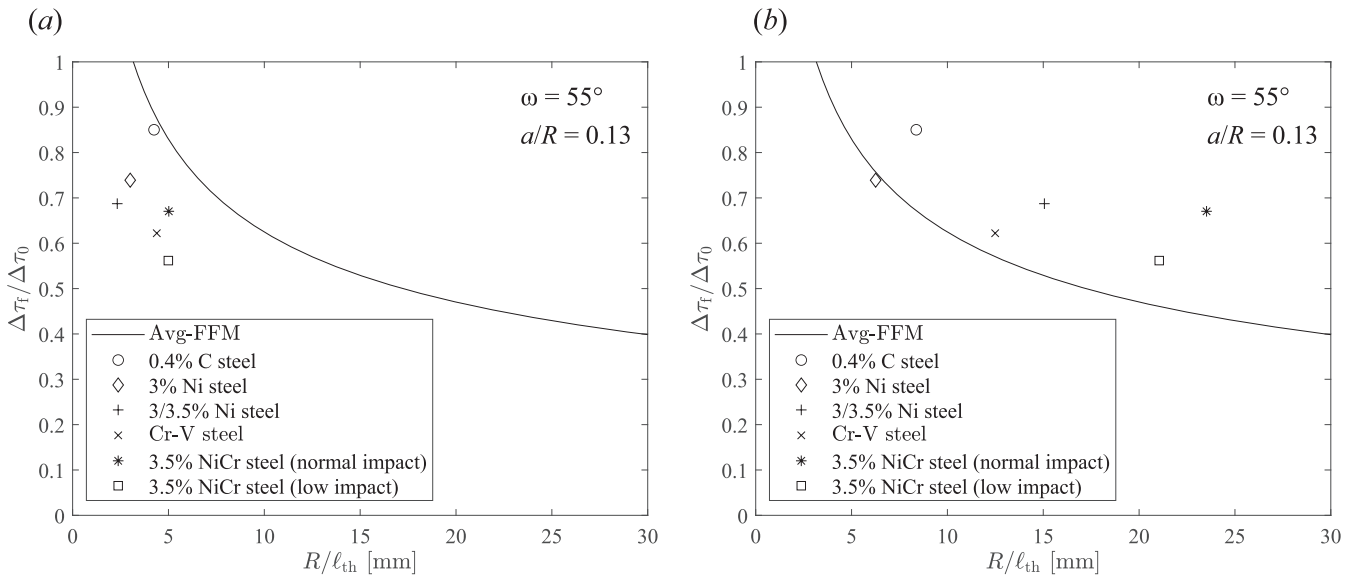


**Fig. 2.** Fatigue endurance limit predictions obtained through the avg-FFM approach for pure mode III as a function of $R/\ell_{th}$, where $\ell_{th} = (\Delta K_{III,th}/\Delta\tau_0)^2$ represents the mode III threshold crack length. In Fig. 2a, the material properties exploited by Susmel and Taylor [76] are implemented while in Fig. 2b the material properties estimated by Campagnolo and Sapora [14] are considered.

[79] loading conditions, with a phase angle between axial/bending and torsion loadings $\varphi = 90°$. Specifically, Berto et al. [83] tested samples made of 39NiCrMo3 steel. Berto et al. [84] generated data for a cast iron grade EN-GJS400, while Berto et al. [22] and Meneghetti et al. [79] tested samples made of titanium alloy Ti-6Al-4 V. In these studies, fatigue endurance limits were assessed at $2\bullet10^6$ cycles and the value of the high-cycle NSIF range $\Delta K_{IA}$ was determined at $N_A = 2\bullet10^6$ cycles by testing 90° V-notched bars under axial/bending fatigue loading. For these materials, to implement the FFM approach, the value of $\Delta K_{I,th}$ was considered equal to $\Delta K_{IA}$, assuming the crack case equivalent to the sharp V-notch case with $\omega = 90°$ under mode I loading.

Atzori et al. [20] conducted tests on 90° V-notched bars made of C40 carbon steel (in a normalized state), under both in-phase ($\varphi = 0°$) and out-of-phase ($\varphi = 90°$) axial-torsion loading conditions. These samples are characterized by a larger value of the notch root radius $\rho = 0.5$ mm compared to the other datasets under consideration. Fatigue endurance limits were evaluated at $2\bullet10^6$ cycles, while neither $\Delta K_{I,th}$ nor $\Delta K_{IA}$ were reported in the original paper. The value of $\Delta K_{IA}$ was thus evaluated through Eq. (9a) by considering the uniaxial fatigue endurance limit of the V-notched bar at $2\bullet10^6$ cycles. Considering the assumption adopted before, $\Delta K_{I,th}$ was set equal to $\Delta K_{IA}$, assuming the crack case equivalent to the sharp V-notch case.

Finally, Pedranz et al. [85] generated axial-torsion fatigue data related to three different cast iron grades: (i) EN-GJS-600 with pearlitic matrix, (ii) EN-GJS-450 with ferritic matrix and high Si continent and (ii) EN-GJS-400 with ferritic-pearlitic matrix. They tested V-notched bars (with $\omega = 60°$ and $\rho = 0.2$ mm or $\omega = 90°$ and $\rho = 0.1$ mm) under both in-phase ($\varphi = 0°$) and out-of-phase ($\varphi = 90°$) multiaxial loading conditions. Regarding the samples made of EN-GJS-600 and EN-GJS-450, axial fatigue endurance limits were assessed at $5\bullet10^6$ cycles whereas the torsional fatigue endurance limits were evaluated at $3\bullet10^6$ cycles. Considering instead the cast iron grade EN-GJS-400, axial fatigue endurance limits of plain and notched samples were evaluated at $3\bullet10^6$ and $2\bullet10^6$ cycles, respectively. Similarly, torsional fatigue endurance limits of plain and notched samples were assessed at $2\bullet10^6$ and $5\bullet10^6$ cycles, respectively. To implement the FFM approach, the value of $\Delta K_{I,th}$ was determined by computing the NSIF range $\Delta K_{IA}$ using Eq. (9a) assuming the crack case equivalent to the sharp V-notch case, as discussed previously.

The deviations between fatigue endurance limit predictions provided by the FFM and avg-FFM approaches defined by Eqs. (4) and (5), respectively, and experimental results, are reported in the last two columns of Table 2. The ratio between the critical crack advancement $\ell_c$ and the net section radius $R$ ranges between 0.01 and 0.09 for the FFM approach and between 0.03 and 0.3 for the avg-FFM method. These values of $\ell_c/R$ confirm that the theoretical approaches can be implemented by using the asymptotic expressions of the stress field and SIF ranges, as $\ell_c$ is considerably smaller than $R$.

The agreement between FFM fatigue predictions and experimental data is deemed satisfactory, considering the many engineering assumptions underlying the FFM approaches and the approximations involved in determining $\Delta K_{I,th}$ and $\Delta K_{III,th}$ values. Deviations are generally under 35 % and more conservative predictions are provided by the avg-FFM approach. This proves that the presented semi-analytical approach is a reliable tool for obtaining fatigue life predictions for different sharply V-notched bars ($0.13 \le a/R \le 1$ and $35° \le \omega \le 90°$) made of several materials (500 MPa $\le \sigma_{UTS} \le$ 1224 MPa) under different multiaxial loading conditions ($0.53 \le \Delta\sigma_{f,exp}/\Delta\tau_{f,exp} \le 8.20$). Furthermore, we observed good agreement between fatigue strength predictions and experimental results for both in-phase ($\varphi = 0°$) and out-of-phase ($\varphi = 90°$) loading conditions. However, it is important to note that for some datasets, especially for those generated by Gough and Pollard [23], the FFM approach defined by Eq. (4) shows deviations greater than 40%. These discrepancies can be explained by the adopted assumptions, which are simplistic and do not fully account for all the physical phenomena influencing the multiaxial fatigue process. Furthermore, it is worth noting that in previous studies the experimental data provided by Gough and Pollard [23] were analyzed also in previous studies, such as Refs. [76,86] where a linear elastic approach has been adopted. More in detail, Ref. [76] was focused only on torsional fatigue endurance limits and maximum deviations between theoretical estimates and experimental data were between 30–35 %, while reduced deviations were obtained in Ref. [86] since the material properties required to apply the fatigue approach were fitted on the experimental results with the aim of minimizing the deviations. A fitting of the material properties on the experimental results has not been performed in this work to apply the FFM, therefore the deviations between theoretical estimates and experimental data remained rather high.

## 6. Conclusions

This work introduced a novel implementation of the FFM coupled criterion to investigate fatigue endurance limits in sharply V-notched bars under combined axial/bending and torsional loading conditions. According to the FFM approach, both a stress condition and an energy balance have to be simultaneously fulfilled to assess the fatigue strength. In this study, the fracture was supposed to initiate along the notch bisector plane with a circumferential-shaped crack. Moreover, to implement the FFM criterion, we considered the threshold value of the mode III SIF range $\Delta K_{III,th}$ equal to $\Delta K_{I,th}$. These hypotheses were thoroughly discussed. A semi-analytical implementation of the FFM approach was then presented. Fatigue life predictions were compared with a large dataset comprehensive of experimental results related to several metals (500 MPa $\leq \sigma_{UTS} \leq$ 1224 MPa). Different V-notched structures were considered, presenting an opening angle $\omega$ ranging between 35° and 90° and a ratio between the notch depth and the net-radius $a/R$ varying between 0.13 and 1. This comparison proved that the FFM approach can provide accurate fatigue endurance limit predictions for different multiaxial loading conditions, under both in-phase and out-of-phase loading conditions. Although the assumptions adopted are simplified and do not fully capture all the physical phenomena affecting the multiaxial fatigue process, e.g. plasticity, friction between crack faces, and mode I crack branching, the model demonstrates its reliability as a tool for obtaining semi-analytical fatigue life predictions, which are valuable for engineering design practice.

## CRediT authorship contribution statement

**Francesco Ferrian:** Writing – review & editing, Writing – original draft, Visualization, Validation, Software, Resources, Methodology, Investigation, Data curation, Conceptualization. **Alberto Campagnolo:** Writing – review & editing, Supervision, Data curation, Conceptualization. **Alberto Sapora:** Writing – review & editing, Supervision, Data curation, Conceptualization.

## Declaration of competing interest

The authors declare that they have no known competing financial interests or personal relationships that could have appeared to influence the work reported in this paper.

## Appendix A

Shape function $k_1(\omega, a/R)$ values of the notch stress intensity factor (NSIF) range $\Delta K_I^V$, considering axial loading conditions, for different values of the opening angle $\omega$ ranging between 15° and 90° and for $0 < a/R_{gross} < 0.9$. These values are obtained in agreement with the NSIF notation defined in Eq. (7a).

**Table A1**
$k_1(\omega, a/R)$ from Noda and Takase [52].

| | | $\omega = 15°$ | $\omega = 30°$ | $\omega = 45°$ | $\omega = 60°$ | $\omega = 90°$ |
|---|---|---|---|---|---|---|
| $a/R_{gross}$ | $a/R$ | $k_1(\omega,a/R)$ | $k_1(\omega,a/R)$ | $k_1(\omega,a/R)$ | $k_1(\omega,a/R)$ | $k_1(\omega,a/R)$ |
| → 0 | → 0 | 1.9927 | 2.0026 | 2.0244 | 2.0563 | 2.1371 |
| 0.01 | 0.0101 | 1.9668 | 1.9705 | 1.9880 | 2.0213 | 2.1051 |
| 0.02 | 0.0204 | 1.9389 | 1.9465 | 1.9657 | 1.9946 | 2.0752 |
| 0.05 | 0.0526 | 1.8532 | 1.8624 | 1.8807 | 1.9082 | 1.9811 |
| 0.1 | 0.1111 | 1.7078 | 1.7142 | 1.7309 | 1.7561 | 1.8208 |
| 0.2 | 0.2500 | 1.4447 | 1.4519 | 1.4677 | 1.4888 | 1.5430 |
| 0.3 | 0.4286 | 1.2209 | 1.2296 | 1.2430 | 1.2605 | 1.3079 |
| 0.4 | 0.6667 | 1.0322 | 1.0393 | 1.0507 | 1.0672 | 1.1070 |
| 0.5 | 1.0000 | 0.8688 | 0.8751 | 0.8847 | 0.8986 | 0.9275 |
| 0.6 | 1.5000 | 0.7231 | 0.7269 | 0.7349 | 0.7464 | 0.7801 |
| 0.7 | 2.3333 | 0.5848 | 0.5868 | 0.5952 | 0.6046 | 0.6369 |
| 0.8 | 4.0000 | 0.4484 | 0.4506 | 0.4555 | 0.4647 | 0.4980 |
| 0.9 | 9.0000 | 0.2975 | 0.3024 | 0.3057 | 0.3126 | 0.3441 |

## Appendix B

Shape function $k_1(\omega, a/R)$ values of the notch stress intensity factor (NSIF) range $\Delta K_I^V$, considering bending loading conditions, for different values of the opening angle $\omega$ ranging between 15° and 90° and for $0 < a/R_{gross} < 0.9$. These values are obtained in agreement with the NSIF notation defined in Eq. (7a).

**Table B1**
$k_1(\omega, a/R)$ from Noda and Takase [52].

| | | $\omega = 15°$ | $\omega = 30°$ | $\omega = 45°$ | $\omega = 60°$ | $\omega = 90°$ |
|---|---|---|---|---|---|---|
| $a/R_{gross}$ | $a/R$ | $k_1(\omega,a/R)$ | $k_1(\omega,a/R)$ | $k_1(\omega,a/R)$ | $k_1(\omega,a/R)$ | $k_1(\omega,a/R)$ |
| → 0 | → 0 | 1.9927 | 2.0026 | 2.0244 | 2.0563 | 2.1371 |
| 0.02 | 0.0204 | 1.8732 | 1.8784 | 1.8969 | 1.9267 | 2.0089 |
| 0.05 | 0.0526 | 1.7317 | 1.7402 | 1.7572 | 1.7828 | 1.8508 |
| 0.1 | 0.1111 | 1.5244 | 1.5260 | 1.5447 | 1.5669 | 1.6221 |
| 0.2 | 0.2500 | 1.2116 | 1.2176 | 1.2288 | 1.2441 | 1.2844 |
| 0.3 | 0.4286 | 0.9864 | 0.9913 | 0.9981 | 1.0117 | 1.0472 |
| 0.4 | 0.6667 | 0.8130 | 0.8150 | 0.8219 | 0.8328 | 0.8655 |
| 0.5 | 1.0000 | 0.6716 | 0.6729 | 0.6802 | 0.6889 | 0.7224 |

(continued on next page)

**Table B1** (*continued*)

| | | $\omega = 15°$ | $\omega = 30°$ | $\omega = 45°$ | $\omega = 60°$ | $\omega = 90°$ |
|---|---|---|---|---|---|---|
| 0.6 | 1.5000 | 0.5500 | 0.5527 | 0.5587 | 0.5675 | 0.6005 |
| 0.7 | 2.3333 | 0.4424 | 0.4446 | 0.4494 | 0.4565 | 0.4915 |
| 0.8 | 4.0000 | 0.3388 | 0.3404 | 0.3442 | 0.3516 | 0.3825 |
| 0.9 | 9.0000 | 0.2252 | 0.2263 | 0.2308 | 0.2365 | 0.2650 |

## Appendix C

Shape functions $k_3(\omega, \eta = a/R)$ proposed by Zappalorto et al. [53], following the NSIF notation defined in Eq. (7b), can be expressed as:

$$\begin{aligned} k_3(30°,\eta) &= 5.2125{\cdot}10^{-4}\eta^{-2} - 2.6341{\cdot}10^{-2}\eta^{-1} + 0.7454 \\ k_3(60°,\eta) &= 3.6731{\cdot}10^{-4}\eta^{-2} - 2.1861{\cdot}10^{-2}\eta^{-1} + 0.8064 \\ k_3(90°,\eta) &= 1.9675{\cdot}10^{-4}\eta^{-2} - 1.5992{\cdot}10^{-2}\eta^{-1} + 0.8718 \\ k_3(120°,\eta) &= 0.1134{\cdot}10^{-4}\eta^{-2} - 0.7964{\cdot}10^{-2}\eta^{-1} + 0.9274 \end{aligned} \tag{B1}$$

These expressions are valid within the range $1/20 \leq \eta \leq 1$. For intermediate opening amplitudes a linear interpolation based on $\lambda_3$ can be considered:

$$k_{3,\omega} = k_{3,\omega_1} + \frac{k_{3,\omega_2} - k_{3,\omega_1}}{\lambda_{3,\omega_2} - \lambda_{3,\omega_1}} \left(\lambda_{3,\omega} - \lambda_{3,\omega_1}\right) \tag{B2}$$

## Data availability

Data will be made available on request.

## References


[1] Leguillon D. Strength or toughness? A criterion for crack onset at a notch. Eur J Mech - A/Solids 2002;21:61–72. https://doi.org/10.1016/S0997-7538(01)01184-6.

[2] Cornetti P, Pugno N, Carpinteri A, Taylor D. Finite fracture mechanics: a coupled stress and energy failure criterion. Eng Fract Mech 2006;73:2021–33. https://doi.org/10.1016/j.engfracmech.2006.03.010.

[3] Taylor D. The Theory of Critical Distances. London: Elsevier; 2007. doi: 10.1016/B978-0-08-044478-9.X5000-5.

[4] Susmel L. Multiaxial notch fatigue. Oxford: Woodhead Publishing; 2009.

[5] Carpinteri A, Cornetti P, Pugno N, Sapora A, Taylor D. A finite fracture mechanics approach to structures with sharp V-notches. Eng Fract Mech 2008;75:1736–52. https://doi.org/10.1016/j.engfracmech.2007.04.010.

[6] Carpinteri A, Cornetti P, Pugno N, Sapora A. On the most dangerous V-notch. Int J Solids Struct 2010;47:887–93. https://doi.org/10.1016/j.ijsolstr.2009.11.017.

[7] Mittelman B, Yosibash Z. Energy release rate cannot predict crack initiation orientation in domains with a sharp V-notch under mode III loading. Eng Fract Mech 2015;141:230–41. https://doi.org/10.1016/j.engfracmech.2015.05.008.

[8] Bathias C, Paris P. Gigacycle Fatigue in Mechanical Practice. CRC Press; 2005.

[9] Sakai T. Review and prospects for current studies on very high cycle fatigue of metallic materials for machine structural use. J Solid Mech Mater Eng 2009;3:425–39. https://doi.org/10.1299/jmmp.3.425.

[10] Liu Y, Deng C, Gong B. Discussion on equivalence of the theory of critical distances and the coupled stress and energy criterion for fatigue limit prediction of notched specimens. 105326 Int J Fatigue 2020;131. https://doi.org/10.1016/j.ijfatigue.2019.105326.

[11] Sapora A, Cornetti P, Campagnolo A, Meneghetti G. Fatigue limit: crack and notch sensitivity by finite fracture mechanics. 102407 Theor Appl Fract Mech 2020;105. https://doi.org/10.1016/j.tafmec.2019.102407.

[12] Sapora A, Cornetti P, Campagnolo A, Meneghetti G, Sapora A, Cornetti P, et al. Mode I fatigue limit of notched structures: a deeper insight into finite fracture mechanics. Int J Fract 2021;227:1–13. https://doi.org/10.1007/s10704-020-00488-6.

[13] Ferrian F, Chao Correas A, Cornetti P, Sapora A. Size effects on spheroidal voids by finite fracture mechanics and application to corrosion pits. Fatigue Fract Eng Mater Struct 2023;46:875–85. https://doi.org/10.1111/ffe.13902.

[14] Campagnolo A, Sapora A. A FFM analysis on mode III static and fatigue crack initiation from sharp V-notches. 108063 Eng Fract Mech 2021;258. https://doi.org/10.1016/j.engfracmech.2021.108063.

[15] Socie DF, Marquis GB. Multiaxial fatigue. Soc Automotive Eng 2000.

[16] Brown MW, Miller KJ. A theory for fatigue failure under multiaxial stress-strain conditions. Proc Inst Mech Eng 1973;187:745–55. https://doi.org/10.1243/PIME_PROC_1973_187_161_02.

[17] Brown M, Miller K. Two Decades of Progress in the Assessment of Multiaxial Low-Cycle Fatigue Life. Low-Cycle Fatigue Life Predict. In: ASTM International100 Barr Harbor Drive, PO Box C700, West Conshohocken, PA 19428-2959; 1982, p. 482–99. doi: 10.1520/STP32442S.

[18] Fatemi A, Socie DF. A critical plane approach to multiaxial fatigue damage including out-of-phase loading. Fatigue Fract Eng Mater Struct 1988;11:149–65. https://doi.org/10.1111/j.1460-2695.1988.tb01169.x.

[19] Morrow J. Cyclic Plastic Strain Energy and Fatigue of Metals. Intern. Frict. Damping, Cycl. Plast., 100 Barr Harbor Drive, PO Box C700, West Conshohocken, PA 19428-2959: ASTM International; n.d., p. 45-45–43. doi: 10.1520/STP43764S.

[20] Atzori B, Berto F, Lazzarin P, Quaresemin M. Multi-axial fatigue behaviour of a severely notched carbon steel. Int J Fatigue 2006;28:485–93. https://doi.org/10.1016/j.ijfatigue.2005.05.010.

[21] Berto F, Lazzarin P, Marangon C. Fatigue strength of notched specimens made of 40CrMoV13.9 under multiaxial loading. Mater Des 2014;54:57–66. https://doi.org/10.1016/j.matdes.2013.08.013.

[22] Berto F, Campagnolo A, Lazzarin P. Fatigue strength of severely notched specimens made of Ti–6Al–4V under multiaxial loading. Fatigue Fract Eng Mater Struct 2015;38:503–17. https://doi.org/10.1111/ffe.12272.

[23] Gough HJ, Pollard HV. The strength of metals under combined alternating stresses. Proc Inst Mech Eng 1935;131:3–103. https://doi.org/10.1243/PIME_PROC_1935_131_008_02.

[24] Lee SB. Multiaxial Fatigue. PA: American Society for Testing and Materials; 1985.

[25] Dang-Van K. Macro-Micro Approach in High-Cycle Multiaxial Fatigue. Adv. Multiaxial Fatigue, ASTM International100 Barr Harbor Drive, PO Box C700, West Conshohocken, PA 19428-2959; 1993, p. 120–30. doi: 10.1520/STP24799S.

[26] Papadopoulos IV. A high-cycle fatigue criterion applied in biaxial and triaxial out-of-phase stress conditions. Fatigue Fract Eng Mater Struct 1995;18:79–91. https://doi.org/10.1111/j.1460-2695.1995.tb00143.x.

[27] Findley WN. A theory for the effect of mean stress on fatigue of metals under combined torsion and axial load or bending. J Eng Ind 1959;81:301–5. https://doi.org/10.1115/1.4008327.

[28] Matake T. An explanation on fatigue limit under combined stress. Bull JSME 1977;20:257–63. https://doi.org/10.1299/jsme1958.20.257.

[29] Susmel L, Lazzarin P. A bi-parametric Wöhler curve for high cycle multiaxial fatigue assessment. Fatigue Fract Eng Mater Struct 2002;25:63–78. https://doi.org/10.1046/j.1460-2695.2002.00462.x.

[30] McDiarmid DL. A general criterion for high cycle multiaxial fatigue failure. Fatigue Fract Eng Mater Struct 1991;14:429–53. https://doi.org/10.1111/j.1460-2695.1991.tb00673.x.

[31] Carpinteri A, Spagnoli A. Multiaxial high-cycle fatigue criterion for hard metals. Int J Fatigue 2001;23:135–45. https://doi.org/10.1016/S0142-1123(00)00075-X.

[32] Liu Y, Mahadevan S. Multiaxial high-cycle fatigue criterion and life prediction for metals. Int J Fatigue 2005;27:790–800. https://doi.org/10.1016/j.ijfatigue.2005.01.003.

[33] Pons AJ, Karma A. Helical crack-front instability in mixed-mode fracture. Nature 2010;464:85–9. https://doi.org/10.1038/nature08862.

[34] Sommer E. Formation of fracture 'lances' in glass. Eng Fract Mech 1969;1:539–46. https://doi.org/10.1016/0013-7944(69)90010-1.

[35] Knauss WG. An observation of crack propagation in anti-plane shear. Int J Fract Mech 1970;6:183–7. https://doi.org/10.1007/BF00189825.

[36] Vojtek T, Pippan R, Hohenwarter A, Holáň L, Pokluda J. Near-threshold propagation of mode II and mode III fatigue cracks in ferrite and austenite. Acta Mater 2013;61:4625–35. https://doi.org/10.1016/j.actamat.2013.04.033.

[37] Vojtek T, Hohenwarter A, Pippan R, Pokluda J. Experimental evidence of a common local mode II growth mechanism of fatigue cracks loaded in modes II, III and II + III in niobium and titanium. Int J Fatigue 2016;92:470–7. https://doi.org/10.1016/j.ijfatigue.2016.02.042.

[38] Younes AI, Engelder T. Fringe cracks: Key structures for the interpretation of the progressive Alleghanian deformation of the Appalachian plateau. Geol Soc Am Bull 1999;111:219–39. https://doi.org/10.1130/0016-7606(1999)111<0219:FCKSFT>2.3.CO;2.
[39] Hull D. The effect of mixed mode I/III on crack evolution in brittle solids. Int J Fract 1995;70:59–79. https://doi.org/10.1007/BF00018136.
[40] Buchholz F-G, Chergui A, Richard HA. Fracture analyses and experimental results of crack growth under general mixed mode loading conditions. Eng Fract Mech 2004;71:455–68. https://doi.org/10.1016/S0013-7944(03)00015-8.
[41] Lazarus V, Buchholz F-G, Fulland M, Wiebesiek J. Comparison of predictions by mode II or mode III criteria on crack front twisting in three or four point bending experiments. Int J Fract 2008;153:141–51. https://doi.org/10.1007/s10704-008-9307-2.
[42] Pham KH, Ravi-Chandar K. On the growth of cracks under mixed-mode I + III loading. Int J Fract 2016;199:105–34. https://doi.org/10.1007/s10704-016-0098-6.
[43] Eberlein A, Richard HA, Kullmer G. Facet formation at the crack front under combined crack opening and anti-plane shear loading. Eng Fract Mech 2017;174:21–9. https://doi.org/10.1016/j.engfracmech.2016.12.004.
[44] Cambonie T, Lazarus V. Quantification of the crack fragmentation resulting from mode I+III loading. Procedia Mater Sci 2014;3:1816–21. https://doi.org/10.1016/j.mspro.2014.06.293.
[45] Pham KH, Ravi-Chandar K. Further examination of the criterion for crack initiation under mixed-mode I+III loading. Int J Fract 2014;189:121–38. https://doi.org/10.1007/s10704-014-9966-0.
[46] Yosibash Z, Mittelman B. A 3-D failure initiation criterion from a sharp V-notch edge in elastic brittle structures. Eur J Mech - A/Solids 2016;60:70–94. https://doi.org/10.1016/j.euromechsol.2016.06.003.
[47] Doitrand A, Leguillon D. Numerical modeling of the nucleation of facets ahead of a primary crack under mode I + III loading. Int J Fract 2018;213:37–50. https://doi.org/10.1007/s10704-018-0305-8.
[48] Doitrand A, Leguillon D, Molnár G, Lazarus V. Revisiting facet nucleation under mixed mode I + III loading with T-stress and mode-dependent fracture properties. Int J Fract 2023;242:85–106. https://doi.org/10.1007/s10704-023-00703-0.
[49] Hutchinson JW, Suo Z. Mixed Mode Cracking in Layered Materials, 1991, p. 63–191. doi: 10.1016/S0065-2156(08)70164-9.
[50] Williams ML. Stress singularities resulting from various boundary conditions in angular corners of plates in extension. J Appl Mech 1952;19:526–8. https://doi.org/10.1115/1.4010553.
[51] Qian J, Hasebe N. Property of eigenvalues and eigenfunctions for an interface V-notch in antiplane elasticity. Eng Fract Mech 1997;56:729–34. https://doi.org/10.1016/S0013-7944(97)00004-0.
[52] Noda N-A, Takase Y. Generalized stress intensity factors of V-shaped notch in a round bar under torsion, tension, and bending. Eng Fract Mech 2003;70:1447–66. https://doi.org/10.1016/S0013-7944(02)00115-7.
[53] Zappalorto M, Lazzarin P, Berto F. Elastic notch stress intensity factors for sharply V-notched rounded bars under torsion. Eng Fract Mech 2009;76:439–53. https://doi.org/10.1016/j.engfracmech.2008.11.008.
[54] Norio H, Jiro I. A crack originating from a triangular notch on a rim of a semi-infinite plate. Eng Fract Mech 1978;10:773–82. https://doi.org/10.1016/0013-7944(78)90032-2.
[55] Philipps AG, Karuppanan S, Churchman CM, Hills DA. Crack tip stress intensity factors for a crack emanating from a sharp notch. Eng Fract Mech 2008;75:5134–9. https://doi.org/10.1016/j.engfracmech.2008.08.002.
[56] Livieri P, Tovo R. The use of the JV parameter in welded joints: stress analysis and fatigue assessment. Int J Fatigue 2009;31:153–63. https://doi.org/10.1016/j.ijfatigue.2008.06.007.
[57] Savruk MP, Rytsar PB. A closed approximate solution of a plane problem of the theory of elasticity for a wedge with symmetric crack. In: Panasyuk VV, editor. Fract. Mech. Mater. Strength Struct. [in Ukr., Kamenyar, Lviv: 1999, p. 125–8.
[58] Duan J, Li X, Lei Y. A note on stress intensity factors for a crack emanating from a sharp V-notch. Eng Fract Mech 2012;90:180–7. https://doi.org/10.1016/j.engfracmech.2012.04.023.
[59] Anderson TL. Fracture Mechanics. CRC Press 2017. https://doi.org/10.1201/9781315370293.
[60] ISO. Metallic materials-Fatigue testing-Fatigue crack growth method, London, UK, 2002.
[61] ASTM International. Standard Test Method for Measurement of Fatigue Crack Growth Rates. ASTM Int 2011:49. doi: 10.1520/E0647-15E01.
[62] Herman WA, Hertzberg RW, Jaccard R. A simplified laboratory approach for the prediction of short crack behavior in engineering structures. Fatigue Fract Eng Mater Struct 1988;11:303–20. https://doi.org/10.1111/j.1460-2695.1988.tb01183.x.
[63] Zerbst U, Vormwald M, Pippan R, Gänser H-P, Sarrazin-Baudoux C, Madia M. About the fatigue crack propagation threshold of metals as a design criterion – a review. Eng Fract Mech 2016;153:190–243. https://doi.org/10.1016/j.engfracmech.2015.12.002.
[64] Newman Jr J, Schneider J, Daniel A, McKnight D. Compression pre-cracking to generate near threshold fatigue-crack-growth rates in two aluminum alloys. Int J Fatigue 2005;27:1432–40. https://doi.org/10.1016/j.ijfatigue.2005.07.006.
[65] Newman Jr JC, Ruschau JJ, Hill MR. Improved test method for very low fatigue-crack-growth-rate data. Fatigue Fract Eng Mater Struct 2011;34:270–9. https://doi.org/10.1111/j.1460-2695.2010.01516.x.
[66] Pearson S. Initiation of fatigue cracks in commercial aluminium alloys and the subsequent propagation of very short cracks. Eng Fract Mech 1975;7:235–47. https://doi.org/10.1016/0013-7944(75)90004-1.
[67] Tschegg EK. A contribution to mode III fatigue crack propagation. Mater Sci Eng 1982;54:127–36. https://doi.org/10.1016/0025-5416(82)90037-4.
[68] Tschegg EK. Mode III and Mode I fatigue crack propagation behaviour under torsional loading. J MaterSci 1983;18:1604–14. https://doi.org/10.1007/BF00542053.
[69] Hellier AK, Corderoy DJH, McGirr MB. Some observations on mode III fatigue thresholds. Int J Fract 1985;29:R45–8. https://doi.org/10.1007/BF00125475.
[70] Tong J. Some aspects of fatigue thresholds under mode III and mixed mode III and I loadings. Int J Fatigue 1996;18:279–85. https://doi.org/10.1016/0142-1123(96)00010-2.
[71] Pook LP, Sharples JK. The mode III fatigue crack growth threshold for mild steel. Int J Fract 1979;15:R223–6. https://doi.org/10.1007/BF00019933.
[72] Pook LP. Mixed-mode fatigue crack growth thresholds: a personal historical review of work at the National Engineering Laboratory, 1975–1989. Eng Fract Mech 2018;187:115–41. https://doi.org/10.1016/j.engfracmech.2017.10.028.
[73] Richard HA, Schramm B, Schirmeisen N-H. Cracks on mixed mode loading – theories, experiments, simulations. Int J Fatigue 2014;62:93–103. https://doi.org/10.1016/j.ijfatigue.2013.06.019.
[74] Endo M, Murakami Y. Effects of an artificial small defect on torsional fatigue strength of steels. J Eng Mater Technol 1987;109:124–9. https://doi.org/10.1115/1.3225951.
[75] Murakami Y, Takahashi K, Takada M, Toriyama T. Quantitative evaluation of effect of artificial small defects on torsional fatigue strength. Trans JAPAN Soc Mech Eng Ser A 1998;64:271–7. https://doi.org/10.1299/kikaia.64.271.
[76] Susmel L, Taylor D. A simplified approach to apply the theory of critical distances to notched components under torsional fatigue loading. Int J Fatigue 2006;28:417–30. https://doi.org/10.1016/j.ijfatigue.2005.07.035.
[77] Beretta M. SIF and threshold for small cracks at small notches under torsion. Fatigue Fract Eng Mater Struct 2000;23:97–104. https://doi.org/10.1046/j.1460-2695.2000.00260.x.
[78] Tanaka K. Crack initiation and propagation in torsional fatigue of circumferentially notched steel bars. Int J Fatigue 2014;58:114–25. https://doi.org/10.1016/j.ijfatigue.2013.01.002.
[79] Meneghetti G, Campagnolo A, Berto F, Tanaka K. Notched Ti-6Al-4V titanium bars under multiaxial fatigue: synthesis of crack initiation life based on the averaged strain energy density. Theor Appl Fract Mech 2018;96:509–33. https://doi.org/10.1016/j.tafmec.2018.06.010.
[80] Qilafku G. Fatigue of specimens subjected to combined loading. Role of hydrostatic pressure. Int J Fatigue 2001;23:689–701. https://doi.org/10.1016/S0142-1123(01)00030-5.
[81] Gough HJ. Engineering steels under combined cyclic and static stresses. Proc Inst Mech Eng 1949;160:417–40. https://doi.org/10.1243/PIME_PROC_1949_160_040_02.
[82] Atzori B, Meneghetti G, Susmel L. Material fatigue properties for assessing mechanical components weakened by notches and defects. Fatigue Fract Eng Mater Struct 2005;28:83–97. https://doi.org/10.1111/j.1460-2695.2004.00862.x.
[83] Berto F, Lazzarin P, Yates JR. Multiaxial fatigue of V-notched steel specimens: a non-conventional application of the local energy method. Fatigue Fract Eng Mater Struct 2011;34:921–43. https://doi.org/10.1111/j.1460-2695.2011.01585.x.
[84] Berto F, Lazzarin P, Tovo R. Multiaxial fatigue strength of severely notched cast iron specimens. Int J Fatigue 2014;67:15–27. https://doi.org/10.1016/j.ijfatigue.2014.01.013.
[85] Pedranz M, Fontanari V, Santus C, Lusuardi D, Berto F, Benedetti M. A strain energy density design approach for large cast iron components: from microstructural analysis to multiaxial fatigue response. 107824 Int J Fatigue 2023;175. https://doi.org/10.1016/j.ijfatigue.2023.107824.
[86] Susmel L. A unifying approach to estimate the high-cycle fatigue strength of notched components subjected to both uniaxial and multiaxial cyclic loadings. Fatigue Fract Eng Mater Struct 2004;27:391–411. https://doi.org/10.1111/j.1460-2695.2004.00759.x.